Supporting Information

Nanometrology based control: taming radical grafting reactions with attoliter precision

Baptiste Maillot, Jean-Frédéric Audibert, Fabien Miomandre, Vitor Brasiliense*

Section S1) Materials and Methods

Materials. All commercial chemicals were used without further purification. The diazonium salt solutions were prepared from corresponding anilines (from different suppliers, see Table S1) using sodium nitrite (Acros Organics) in a mix 95 : 5 milli-Q water (18.2 MΩ.cm-1) : DMSO (Carlo Erba Reagents) at stoechiometric proportions. The aqueous phase pH was raised to 2 using a commercial 1M hydrochloric acid solution (Sigma Aldrich).

Compound	Supplier (purity)
$-NO_2$	Sigma Aldrich (98%)
-CN	Acros Organics (98%)
$-NH_2$	Sigma Aldrich (99%)
-OMe	Sigma Aldrich (98%)
-H	TCI Chemicals (>98%)
-CCH	Sigma Aldrich (97%)
-pMe	Sigma Aldrich (99%)
-mMe	Sigma Aldrich (99%)
oMe	Sigma Aldrich (99%)
$-C(CH_3)_3$	Sigma Aldrich (99%)
$-(CH_3)_2$	Sigma Aldrich (99%)
$-C_6H_{13}$	Sigma Aldrich (90%)

Table S1. Suppliers and purity for the different aniline derivatives used to prepare diazonium salts.

Surfaces. Except for the data shown in Section S5a, all grafting operations were conducted over inert borosilicate coverslips (24x60 mm,No 1.5 thickness 170 ± 5 µm, VWR international). For the data shown in Section 5a, ITO slides were purchased from SPI (22 x 40 mm, 170 ± 20 µm thickness, 30-60 Ω). Au slides were prepared by Au evaporation over glass slides. The glass surfaces were cleaned by immersing in isopropanol for 20 min followed by 15 min in UVO Cleaner(Jelight). Au deposition was peformed using a EMITECH K650 sputter coater under argon atmosphere (0.1 mbar) at 60 mA applied for 90 s.The Au layer thickness was controlled by atomic force microscopy, leading to Au layers of 7 ± 1 nm. Such a thin layer still presents enough light transmission through the sample, enabling grafting experiments to be carried out.

Experimental setup and representative photografting data. The experimental setup used to record the grafting curves is indicated below. It is similar to setup previously used by our group. A complete setup description can be found in the Methods section, and in previously reported papers[s1].

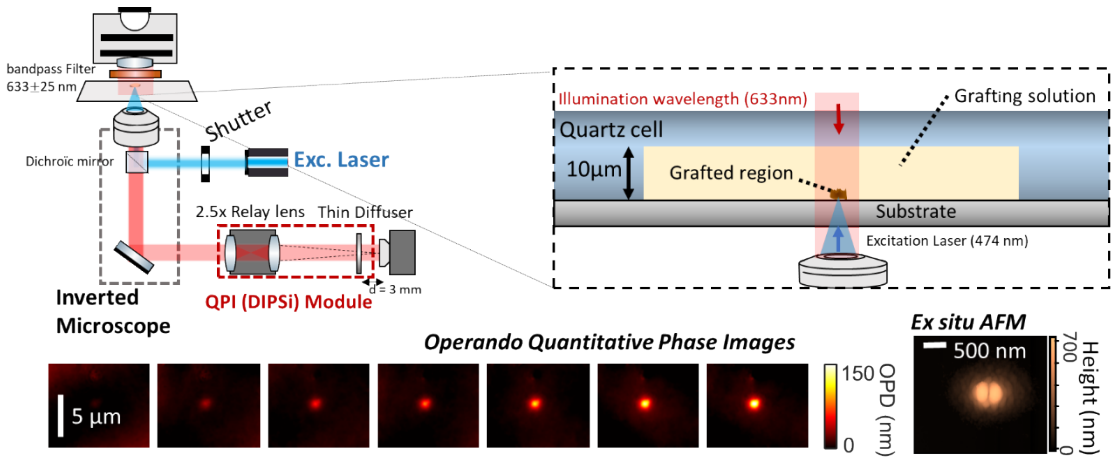

Figure S0. Scheme of the experimental setup, the grafting cell used in this paper, and representative data. The data show the photografting of a aryldiazonium salt with a -C≡CH para substituted moiety, obtained by irradiating a ~ 1µm² zone (45 µW; λ_{exc}= 474 nm) as it will describe collected for the grafting of . The phase images shown in the bottom layer enable the grafting operation to be tracked in operando. After the end of the experiment, the grafted pattern can be further characterized using Atomic force microscopy as indicated in the methods section and illustrated here by the side image. The AFM data reveals the physical volume of the grafted pattern along with morphological details which cannot be resolved through optical techniques

Section S2) Diazotization Kinetics

Diazotization reactions were performed in a 3mL quartz cuvette. All spectra are recorded in a spectrophotometer (Carry 5000, Agilent), in kinetic mode. Spectra are recorded every 30 s at 600 nm/s, starting immediately after addition of the $NaNO_2$ diazotization agent.

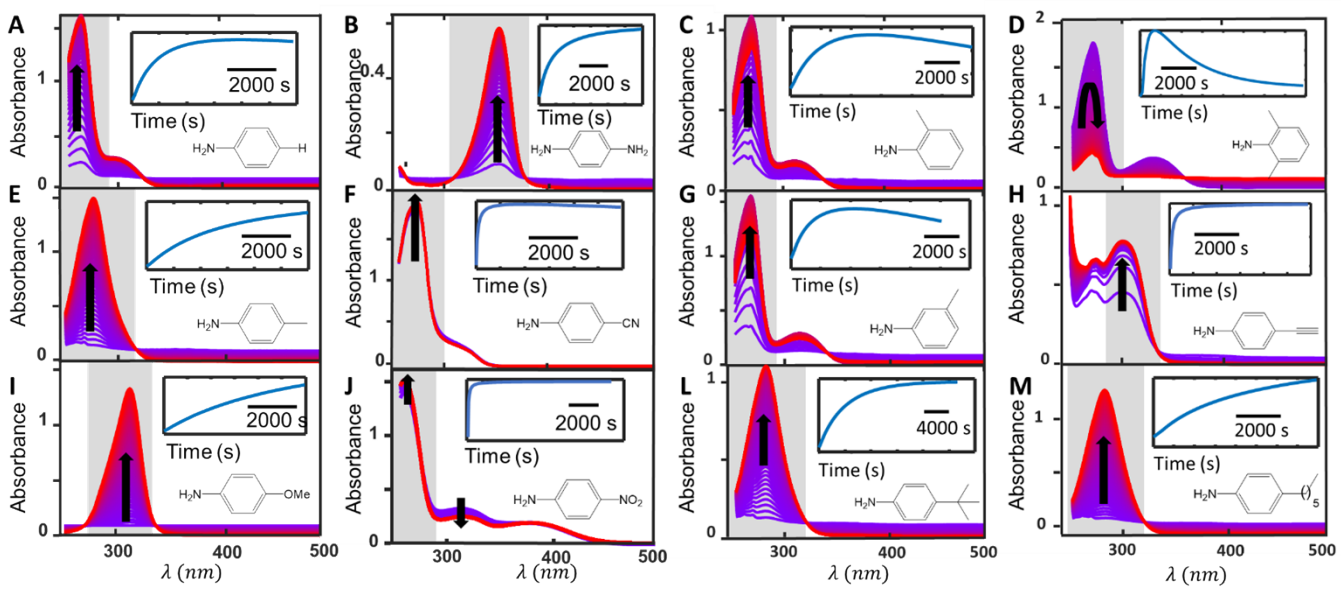

Figure S1. In situ UV-Vis absorption difference spectra of diazotization spectra. The chemical structure of the aniline precursor of each diazotization is shown as an inset, along with the kinetic trace (normalized), obtained by integrating the region of interest (highlighted in gray). All reactions were conducted in a 3 mL quartz cuvette (1 cm optical path), at 200 μM concentration in the presence of equimolar quantities of $NaNO_2$. A mixture H_2O (pH2): DMSO (95:5) is used as the solvent, enabling solubilization of all molecules. The H2O pH is adjusted with HCl. The data shown in Fig. 2 (C,D and L) are repeated here for convenience.

Section S3) Fitting procedure and results

After recording of the spectral data (Fig S1), and integration, we fit the into a simplified two state model (Fig 2 B in the main text). A fully analytical approach for describing such curves is in principle possible, but would require precise knowledge about the absolute molar absorptivity coefficient for the (pure) diazonium species. Instead of carrying out such a time-consuming procedure (which is challenging and even dangerous for relatively unstable diazonium salts[S3,S4]), we design a numerical approach to the problem, described in this section. Our procedure is carried out under the following simplifying hypothesis: (i) The spectra are dominated by the diazonium salt response in the integrated region (indicated by the gray squares in Fig.SI) within the timeframe of the experiments (ii) diazonium degradation is a first order (or pseudo first order) process.
The following system of differential equations describe the simplified system, where [An] describe the aniline concnetration, [NO2-] the nitrite concentration and [Dz] the diazonium salt concentration:

$$\frac{d[An]}{dt} = -k_1[An]\left[NO_2^-\right]$$

$$\frac{d[Dz]}{dt} = k_1[An]\left[NO_2^-\right] - k_d[Dz]$$

$$\frac{d\left[NO_2^-\right]}{dt} = -k_1[An]\left[NO_2^-\right]$$

with initial conditions $[An], \left[NO_2^-\right]$ = C_0 , [Dz] = 0, at t = 0. The system is numerically solved using Matlab's ODE45 solver. In order to compare experimental and simulated kinetic traces, we normalize both curves, removing the unknown absorptivity ε_{Dz} dependency.

The goodness of each fit is evaluated by taking the l^2 norm of the differences between the curves, $r = \sum_i (y_{exp}(ti) - y_{sim}(t_i))^2$, which must be as close to zero as possible. After first manually adjusting the values of k_1 and k_d for minimizing the curves differences, we employ an automated minimization procedure (fmincon) to check for the existence of no other minima of r. The results of the fit for each substituted anilines are shown below.

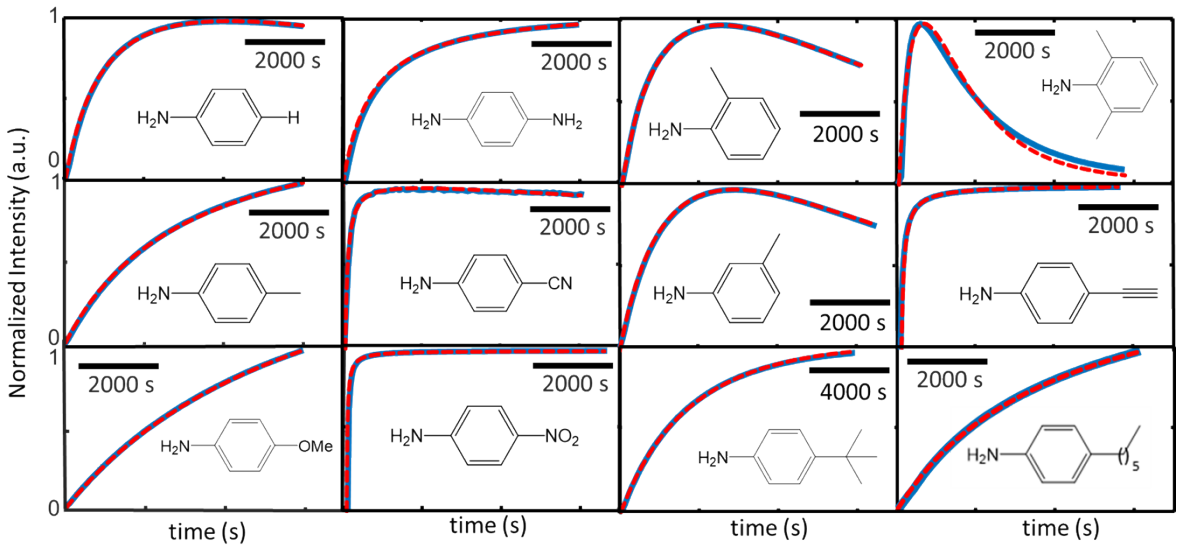

Figure S2. Comparison between the diazotization kinetics traces, obtained by integration of the ROI indicated in gray in fig.S1, and the fit data, leading to the kinetic constants shown in Fig.2 of the main text. All fit residues (l^2 norm) are very small (<1%) compared to te curves, as detailed in the table below.

Aryl radical Precursor	R =		Max)
p-NO_2	9,1	$1{,}4.10^{-1}$	$1{,}7.10^{-2}$
p-CN	2,6	$4{,}5.10^{-2}$	$1{,}5.10^{-2}$
p-NH_2	$9{,}0.10^{-2}$	$1{,}9.10^{-3}$	$1{,}4.10^{-4}$
p-OCH_3	$2{,}1.10^{-2}$	$5{,}8.10^{-4}$	$2{,}6.10^{-5}$
p-H	$2{,}8.10^{-1}$	$5{,}4.10^{-3}$	$9{,}0.10^{-4}$
p-C ≡ CH	8,1	$1{,}4.10^{-1}$	$9{,}1.10^{-3}$
p-CH_3	$2{,}3.10^{-1}$	$5{,}7.10^{-4}$	$1{,}1.10^{-4}$
m-CH_3	$2{,}9.10^{-1}$	$5{,}8.10^{-4}$	$5{,}3.10^{-4}$
o-CH_3	$8{,}4.10^{-2}$	$2{,}0.10^{-5}$	$2{,}3.10^{-4}$
p-$C(CH_3)_3$	$3{,}0.10^{-1}$	$3{,}5.10^{-5}$	$8{,}1.10^{-5}$
o-$(CH_3)_2$	15,4	$5{,}2.10^{-3}$	$7{,}6.10^{-2}$
p-C_6H_{13}	$1{,}2.10^{-1}$	$2{,}3.10^{-5}$	$1{,}9.10^{-4}$

Section S4) Absorption spectra and grafting rates.

This section relates the observed grafting rates and the molar absorption coefficient , showing that the reaction efficiencies can be quite different depending on the substituents on the aryl ring. Grafting rates are calculated from the slope of the linear regime of grafting curves (OVD(t)) , as indicated in the main text. The grafting curves are normalized by the total energy taking measured differences in incident power into consideration. The solutions were realized in a mix of H_2O (pH = 2 adjusted with a 1 M HCl solution) : DMSO (95 : 5) at 5 mM in presence of equimolar quantity of sodium nitrite. The grafting kinetics are recorded using QPI, as described in the main text.

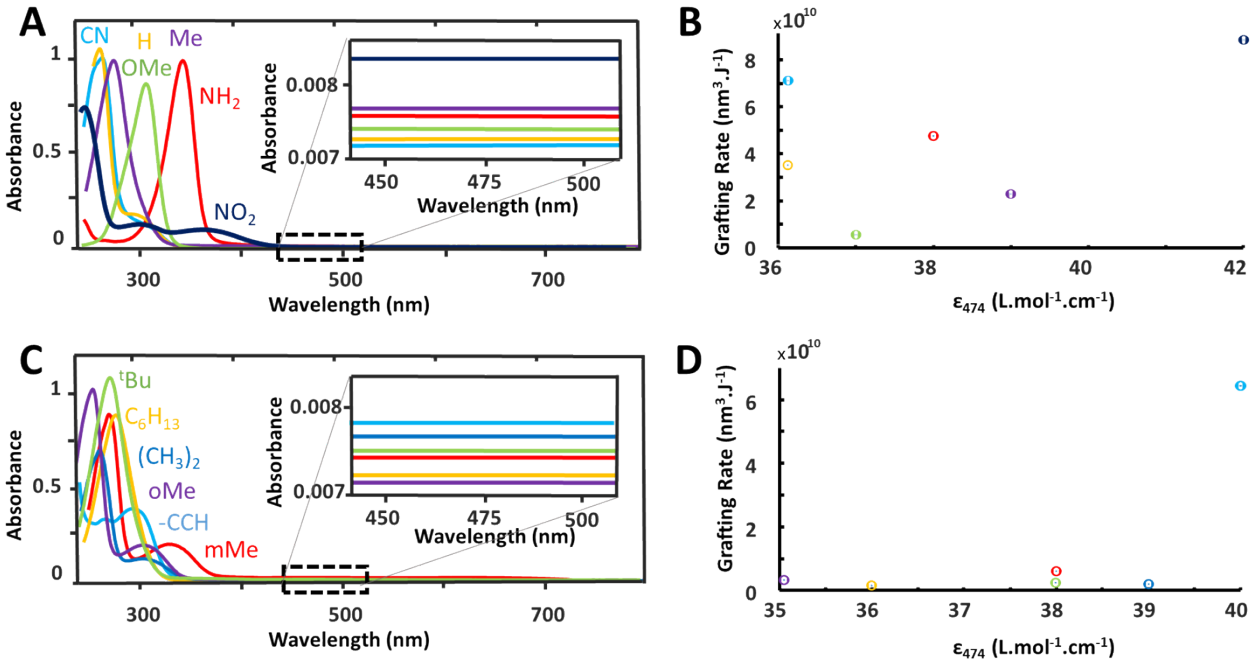

Figure S3. Absorption spectra of diazonium salts used in this paper, split between the electronic (A-B) and steric (C-D) series for clarity. (A,C) Absorption spectra of compounds used in the electronic (A) and steric (C) series (C = 200 µM, in 95:5 H2O(pH2):DMSO, freshly prepared after the diazotization kinetics shown in Fig.S1). The insets zoom in the region used in this paper to excite the grafting reactions (λ_{exc} = 474 nm), showing very weak absorption values. (B,D) Comparison between the observed grafting rates and the molar absorptivity values. Although all species present similar molar absorptivity in the excitation wavelength, very different grafting rates are observed, indicating that substituents on the aryl ring lead to different grafting efficiencies.

Section S5) Influence of the surface in the grafting rate

This section analyzes the influence of the surface material on the grafting rate and efficiency. Three sets of experiments are conducted from 5mM nitrobenzene solutions onto glass slides, on ITO surfaces (ref fabricatn) and on glass slides covered with thin layers (th = 6 ± 1 nm) of gold. As one can see in the Figure, changing the surface properties only significantly impacts the induction regime, as the grafting reaction promptly starts with irradiation in gold and ITO, but is delayed when carried out on glass. After the grafting rate reaches a steady state, no meaningful differences are observed, as indicated in the inset. This behavior is consistent with the assignement of the two grafting regimes, analogous to nucleation and growth. In the inductive regime, generated radicals react with the surface directly, and therefore are afected by the surfaces properties. After the irradiation zone is completely covered with a first organic layer, the the grafting rate is controlled by the efficiency of radical addition onto grafted layers, and the influence of the surface orginal state are expected to be minimal, as indeed observed.

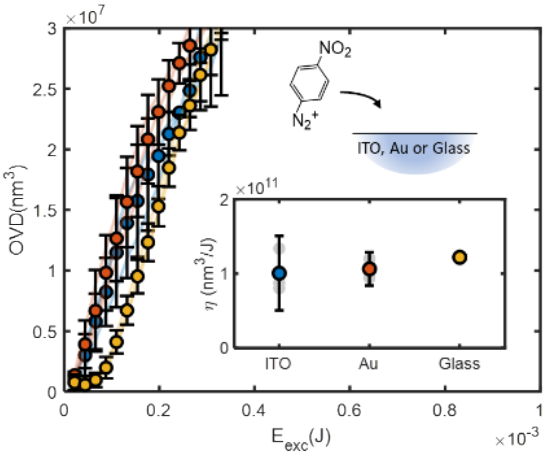

Figure S4. QPI monitoring of grafting operations carried out on different surfaces, showing differences in the inductive regime, but similar steady state behavior for high converages. Solutions of 5mM 4 nitro benzene diazonium were used to collect this dataset, while the laser irradiation of 11 μW was used.

S6) Influence of radical proximal position on grafting rates

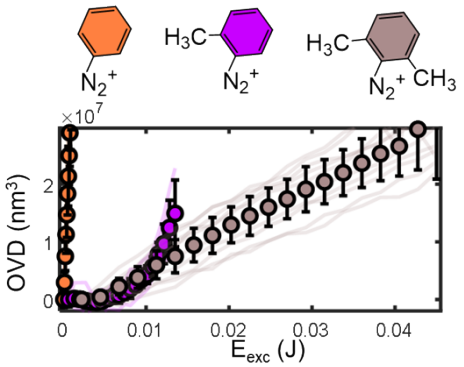

Figure S5 . Grafted volume rate as a function of the excitation energy of three progressively more o substituted diazonium cations. While unsubstituted phenyl radicals are unperturbed and quickly graft onto the surface, o-CH_3 and o-$(CH_3)_2$ are considerably slower. Such general trends, however, elude quantitative descriptions. Indeed, if o-$(CH_3)_2$ initially grafts quicker o-CH_3, the trend reverses for longuer grafting operations, indicating that the nucleation and growth regimes are not affected in the same manner by the o- substitutions.

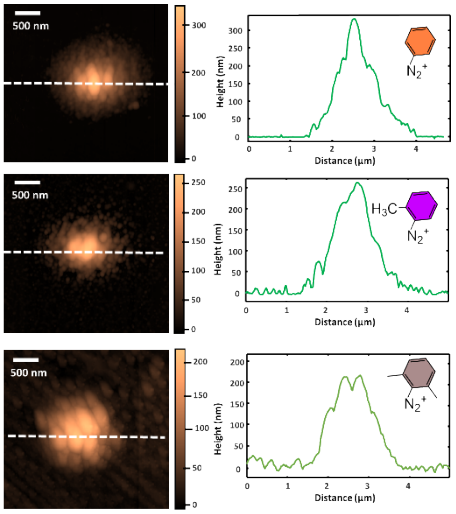

Figure S6. Ex-situ Atomic force microscopy images of typical grafted spots obtained from H-, o-CH3 and o-$(CH3)_2$ substituted diazonium salts, along with profiles extracted from the line indicated by the dashed line. These images were collected after carefully rinsing the modified surface with water and drying under N_2 flow, and demonstrate the stability of grafted patterns.

Section S7) Refractive index evaluation procedure.

The refractive index of grafted layer (n_{layer}) allows transforming the optical path difference (OPD) into the actual thickness of the grafted layer (L), according to eq. 1, in which n_m is the refractive index of the grafting medium:

$$OPD = (n_{layer} - n_m) \times L$$

Integration of the OPD over the grafting zone yields the optical volume difference (OVD), which relates to the actual volume of the grafted layer V by:

$$OVD = (n_{layer} - n_m) \times V$$

n_m is evaluated at the observation wavelength ($\lambda_{obs} =$ 633 nm) using an Abbe refractometer (Bausch & Lomb), leading to the value of 1.335 $\pm$ 0.001 for all grafting solutions. For each aniline precursor, we conduct a large number ($\sim$ 10) of grafting experiments, leading to a series of grafted spots which are later evaluated with the help of an Atomic Force Microscopy measurements. A typical example of sequence of AFM images is indicated in Figure shown below (data collected for the determination of the refractive index of p-CN substituted diazonium salts is shown). After carrying out the grafting operations with simultaneous measurement of OVD, the sample is thoroughly rinsed with water, dried under N_2 flow, and characterized with AFM. The volume of each spot is extracted by numerically integrating the modified zone. The ratio between the OVD and V is used to estimate the material refractive index. Data obtained for several

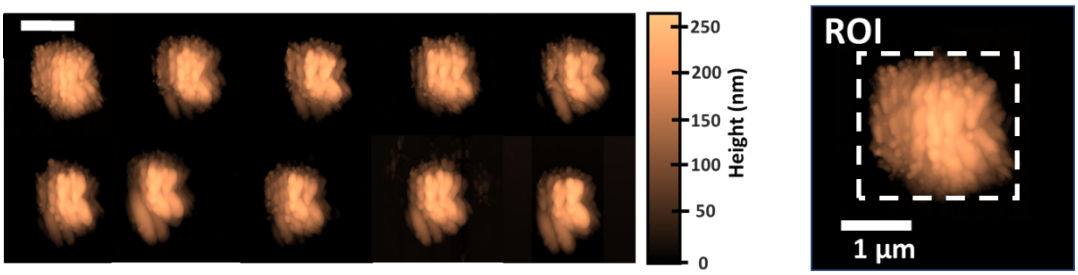

Figure S6. Ex-situ AFM images of a series of 10 patterns obtained from grafting of p-CN-aryldiazonium chloride salt. Each spot is obtained by exciting the formation of aryl radicals in the vicinity of the glass slide, as indicated in the main text.

Substituent	Refractive index (N_{meas})
p-NO_2	1.68 $\pm$ 0.02 (9)
p-CN	1.65 $\pm$ 0.02(10)
p-NH_2	1.41 $\pm$ 0.02(9)
p-OMe	1.41 $\pm$ 0.02(9)
p-H	1.50 $\pm$ 0.03(8)
p-C $\equiv$ CH	1.49 $\pm$ 0.03(9)
p-CH_3	1.46 $\pm$ 0.03(8)
m-CH_3	1.53 $\pm$ 0.02(8)
o-CH_3	1.45 $\pm$ 0.04(7)
p-$C(CH_3)_3$	1.41 $\pm$ 0.03(8)
o-$(CH_3)_2$	1.47 $\pm$ 0.02(8)
p-C_6H_{13}	1.39 $\pm$ 0.04(9)

Table S2. Evaluated refractive index of grafted aryl radicals bearing different substituents, estimated according to the procedure provided in the methods section. Mean values with 3^{σ} errors are indicated, resulting from at least 7 independent estimations. (the actual number for each class is indicated in parenthesis).

Section S8) Grafting data in linear scales

Throughout the paper, all grafting curves are shown in a semi-log scale in order to facilitate visualization. Although practical for such purpose, such scale deforms the grafting curves hiding, for example the transition between exponential and linear growth, which are easier to observe in linear scale. The linear plots are reported here, along with the corresponding diazonium salts structures.

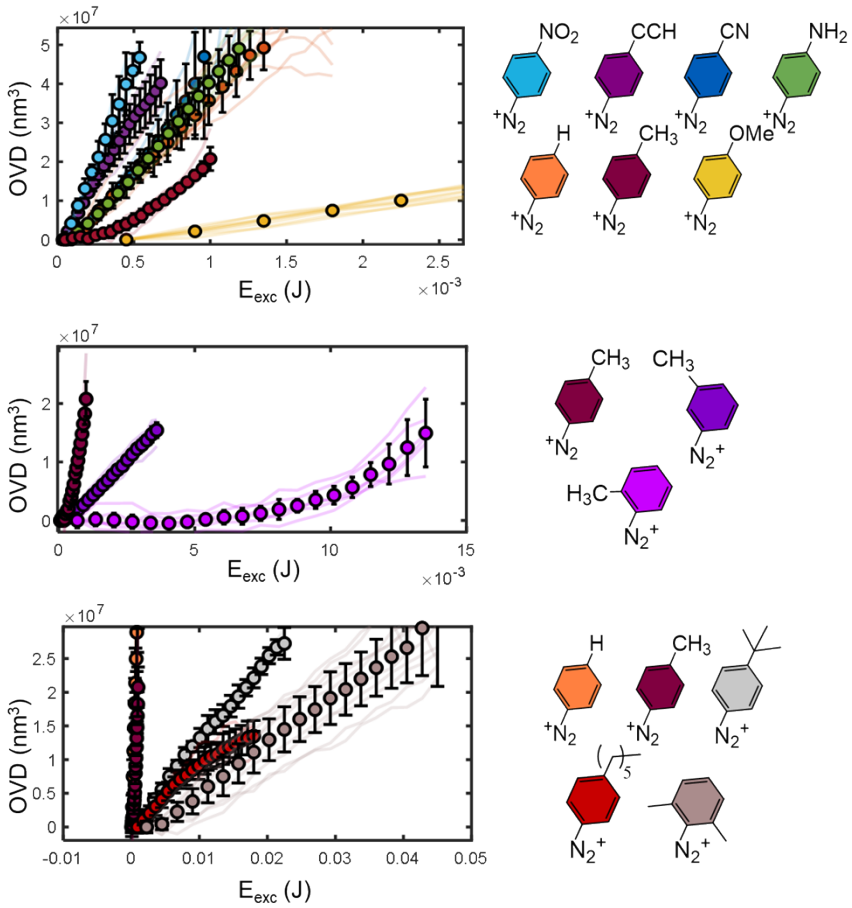

Figure S7 . Grafted volume rate as a function of the excitation energy portrait in a linear scale. The data shown here corresponds to the plots shown in (A) Fig.3and (B,C) Fig.4 of the main text. The linear scale facilitates the observation of the transition between induction and linear regimes (e.g. p-methyl-diazonium in panel A, o-methyl -diazonium in panel B), as well as saturation events, as observed for p-hexyl diazonium in panel C)

Supporting Information References:

[S1] V. Brasiliense, J.-F. Audibert, T. Wu, G. Tessier, P. Berto, F. Miomandre, Small Methods 2022, 6, 2100737.

[S2] P.Berto, H. Rigneault, M. Guillon, *Opt. Lett.* **2017**, *42*, 5117–5120.

[S3] J. D. Firth, I. J. S. Fairlamb, *Org.Lett.* **2020**, *22*, 7057–7059.

[S4] M. Sheng, D. Frurip, D. Gorman, *J. Loss Prev. Process Ind.* **2015**, *38*, 114–118.